SAXION UNIVERSITY OF APPLIED SCIENCES

Technical Research

Smart Solutions Semester 1
2019-2020

Author: Dimitar Rangelov
Version: 0.0.1

Contents

Introduction 2

1. Temperature and Humidity Sensor 3

1.1 Simulations on Humidity domain 3

1.2 Simulations on Temperature domain 4

1.3 Results for Humidity 5

1.4 Results for Temperature 6

1.5 Function Simultaneously of Temperature and Humidity 7

1.6 Hysteresis 7

1.7. Response speed 8

1.8 Testing and evaluating 8

2. Weight Sensor 10

2.1 Load Cell Basics 10

2.1.1 Hydraulic Load Cells 10

2.1.2 Pneumatic Load Cells 11

2.1.3 Strain Gauge Load Cells 11

2.2 Testing and evaluating 12

2.2.1 Reference research 12

2.2.2 Applying the reference research 13

3. Micro controllers 15

3.1 Arduino UNO 15

3.2 Arduino NANO 16

3.3 Arduino DUE 16

3.4 Arduino MEGA 2560 17

3.5 Comparison 17

4. Architecture 18

5. Graphical user interface 19

6. Bibliography 20

Introduction

REV'IT! is a Dutch company, based in Oss, which develops innovative motorcycle clothing since 1995. REV'IT! is a worldwide known company with over a thousand dealers all over the world. After five years REV'IT! introduced the 'Engineered skin design' concept, a new method for product development. A groundbreaking method to deliver higher protective motorcycling products. In 2009 REV'IT! made a license agreement with Gore-Tex. By combining Gore-Tex with the Engineered skin, the performance and safety of the products have improved (REV'IT!, 2019).

REV'IT! makes motorcycle clothing for men and women from 18 years and older. The company creates collections which are divided in three different types of motorcycle garment categories: Sport, Adventure and Urban. These categories are based on the level of performance of the motorcyclist. REV'IT! also provides a lifestyle collection for both men and women.

With the lab located in Oss, REV'IT! tests their own fabrics at their own headquarters. Before the garments are produced the fabrics will first be tested in the lab. The fabrics are tested on their safety level to see if the products fulfill to the standards. Another important factor is to test the materials on the comfort level. REV'IT! aim is to provide protective and comfortable products towards their customers. A few examples of these tests are the tensile strength test, abrasion resistance, dimensional stability and many more. While performing these tests the seam strength, the stretch ability and the wear resistance of the products are for example tested (REV'IT!, 2019).

All information is acknowledged on the 5th of September 2019 by Mr. Memel, the Lab Coordinator at REV'IT! Oss

1. Temperature and Humidity Sensor

The aim of this chapter is to define which sensor is most suitable for the research project. This has been done to up efficiency and the accuracy of the device that will be built.

The sensors are divided on different classes and the priority of this research is mainly sensors that are high class and also has high specification. Because of that the DHT11 and overall the DHT family are clearly a different class of sensor with substantially lower specification and has been dropped from further investigation. In previous tests it performed perfectly well with respect to its specification.

The sensors are mainly from several families and manufactories but with almost same specifications and class. Furthermore will be simulated the eventual behavior in humidity domain and temperature domain separately. After that will be shown the results and the Function Simultaneously of Temperature and Humidity that will represent clearly in 3d the relationship between temperature and humidity and how this affects the sensor by its own.

1.1 Simulations on Humidity domain

In the pictures below are representing the results of the simulation for humidity of each of the sensors. In the first graph is visible that as big is the graph as less accurate and more percent difference has the sensor. And other way around as small is the graph as more accurate is the sensor.

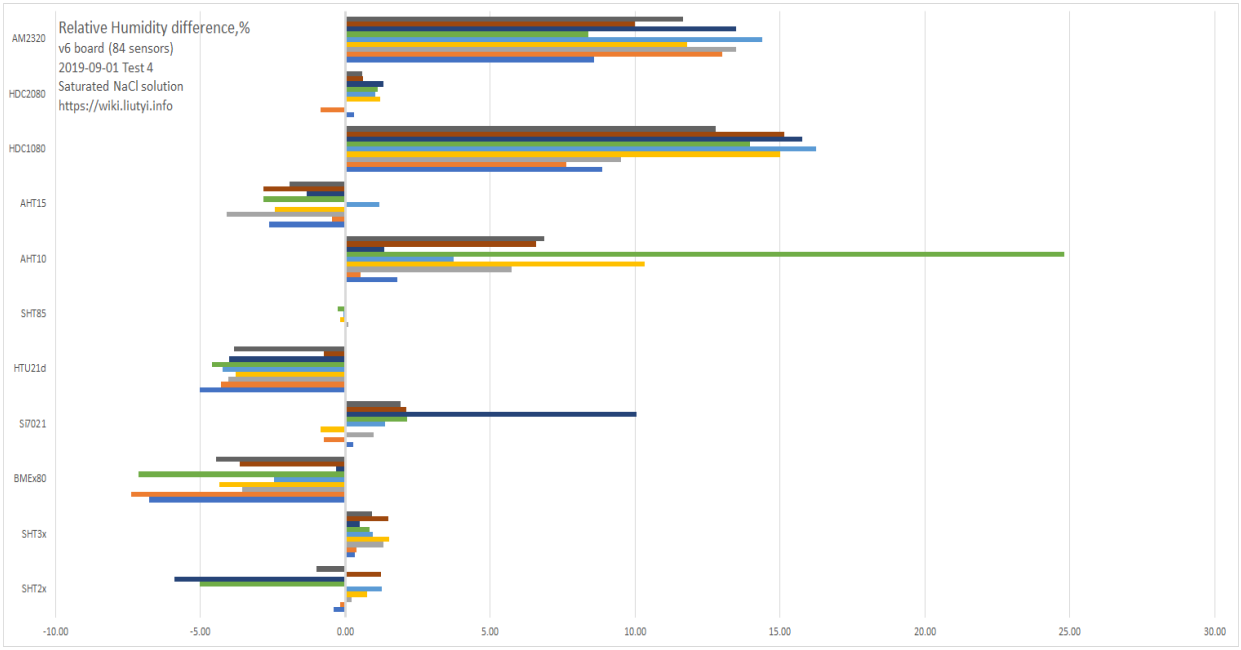

Figure 1 Relative Humidity difference [1]

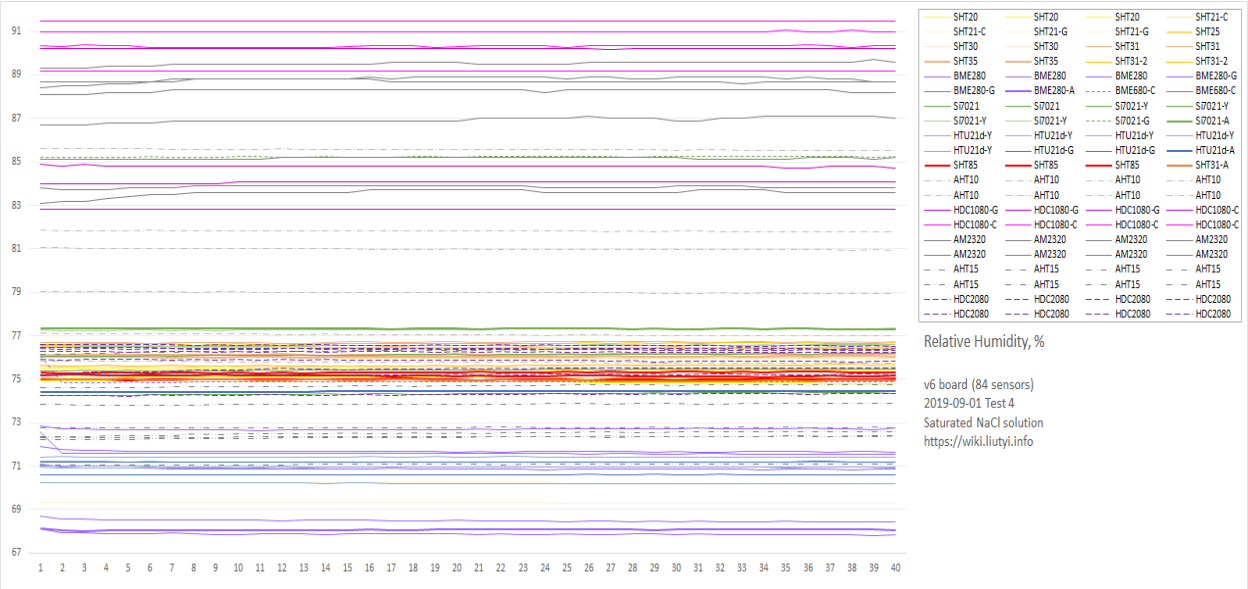

Figure 2 Relative Humidity Sensor [1]

1.2 Simulations on Temperature domain

In the pictures below are representing the results of the simulation for temperature of each of the sensors. In the first graph is visible that as big is the graph as less accurate and more percent difference has the sensor. And other way around as small is the graph as more accurate is the sensor.

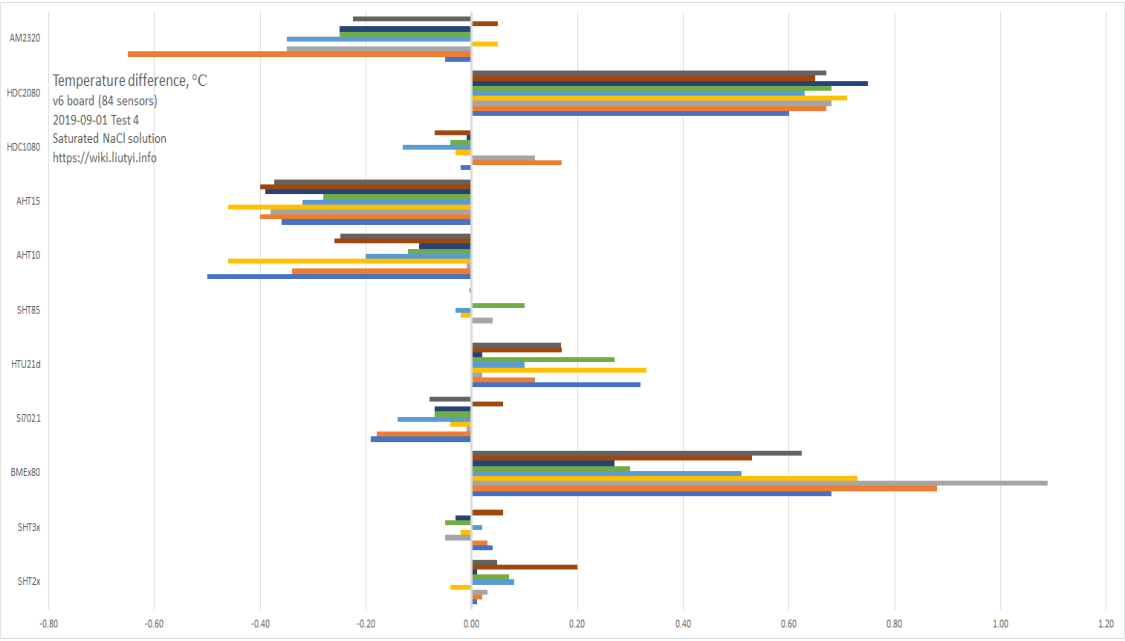

Figure 3 Temperature difference [1]

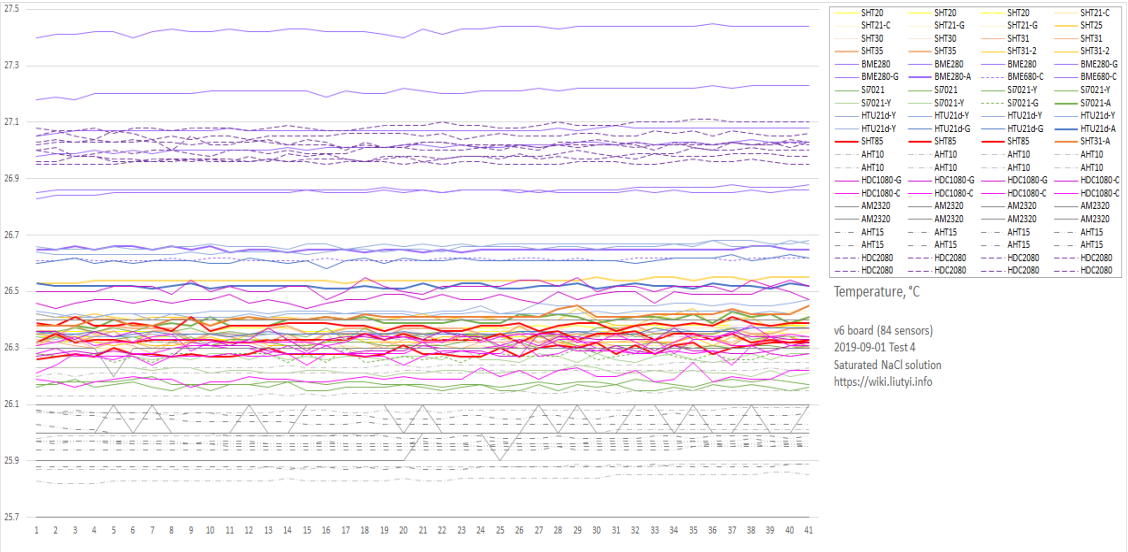

Figure 4 Temperature measurements [1]

1.3 Results for Humidity

` The plot below showing the deviation of humidity values from the known reference value. These plot show the error of each sensor as a function of humidity. The shaded grey region is the specified tolerance from the manufacturers' datasheets. All data collected, irrespective of temperature, are shown as blue dots. Red crosses are just those obtained at 25±1°C, so any that lie above or below the shaded region fail to meet the advertised specification. Where blue dots scatter outside the shaded region it indicates a drift in the calibration as a function of temperature. Red lines are quadratic fits to the 25±1°C data.

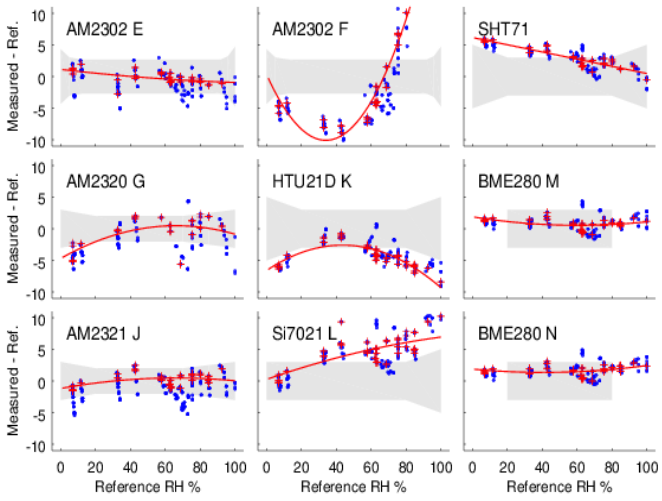

Figure 5 Plots showing the deviation of humidity values from the known reference value. [2]

1.4 Results for Temperature

The plot below is showing in red boxes and a linear fit line are measurements for all sensors with saturated ammonium nitrate over the temperature range 5–35°C. Plotted for comparison are values taken from the published literature. Cyan data from O'Brien (1948) and yellow from Wexler (1954). The thin black line is an equally weighted fit to both. [2]

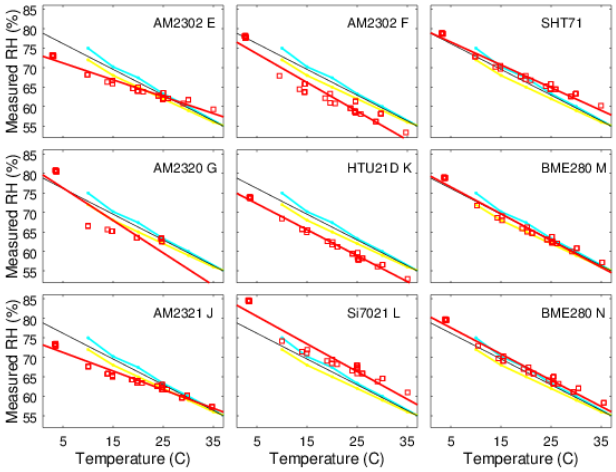

Figure 6 All sensors with saturated ammonium [2]

The plot below is showing as red boxes and a linear fit are measurements for all sensors with saturated magnesium chloride over the temperature range 5–35°C. Plotted for comparison are values taken from the published literature. Blue data are from Greenspan (1977), cyan data from O'Brien (1948), green from Rockland (1960), magenta are the CRC Handbook (1977) and yellow, Wexler (1954). The thin black line is an ensemble fit to them all, weighting all equally. [2]

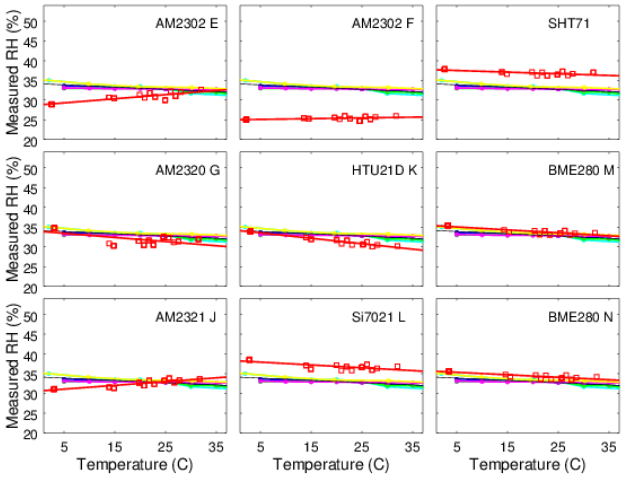

Figure 7 All sensors with saturated magnesium [2]

1.5 Function Simultaneously of Temperature and Humidity

Surfaces are showing deviation of each sensor from the true relative humidity as a function of temperature and humidity. A 'perfect' sensor would be a featureless green-yellow plane at zero. Blue shows low readings and red are high.

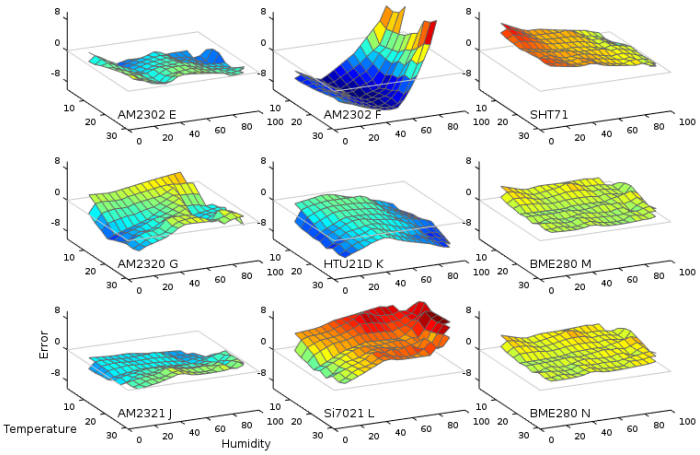

Figure 8 Temperature and Humidity [2]

1.6 Hysteresis

Deviations from the known reference value as humidity is systematically cycled from high to low and back to high. Two complete cycles of 92%, 60%, 33%, 7%, 33%, 60%, 92% are shown. For most sensors the traces followed on rising and falling humidity are reasonably close together, showing little hysteresis bias. A couple of sensors do show a strong effect. (Notes on particular sensors: AM2302 F output saturates at 99.9% for K_2NO_3 so no values are plotted. The AM2321 generally failed to give any output for K_2NO_3. It occaisionally provided an intermittent reading, but largely fails for humidity >90%. The AM2320 generally failed to give any output for NH_4NO_3. It occaisionally provided an intermittent reading, but largely fails for humidities around 50-70%.)

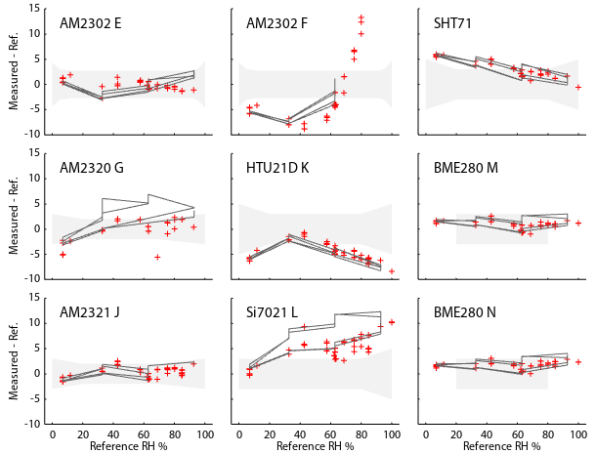

Figure 9 Deviations from the known reference value as humidity is systematically[2]

1.7. Response speed

Time response of the devices when exposed to a sudden upwards and downwards change in humidity. Left panel shows data directly from the sensors. Since the AM23xx devices return a previously cached value, they show the step change with a lag of one data point. In the right hand panel the lag has been arbitrarily removed and the values normalised in order to compare the intrinsic response speed of the sensor elements.

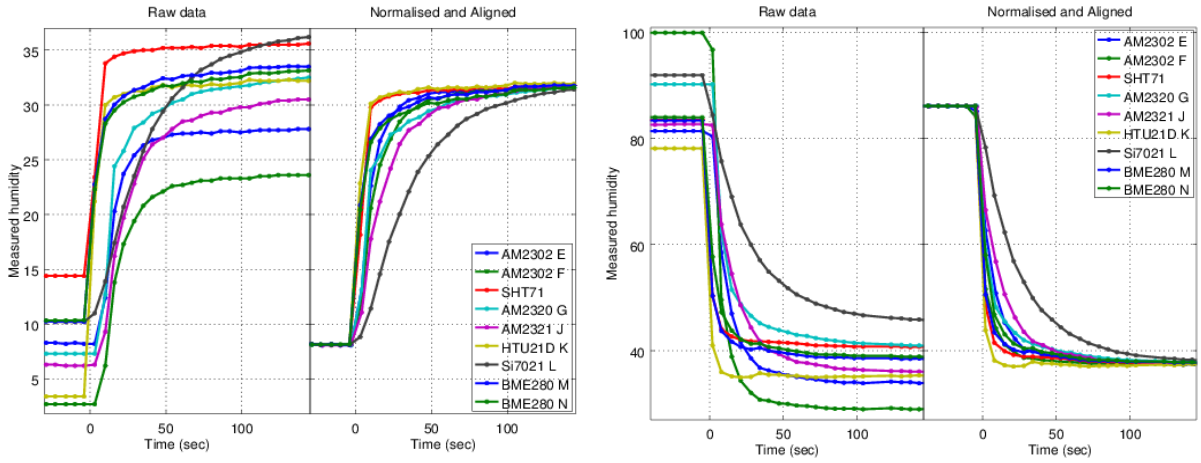

Figure 10 Time response of the devices when exposed to a sudden upwards and downwards change in humidity. [2]

1.8 Testing and evaluating

Overall the SHTxx sensor family is the best for the research project and because of that the final decision was made to be compared SHT31-D and SHT85 in real life situations. In the picture below are shown the inner of both of the sensors. In the left part is SHT85 and in the right side is SHT31-D.

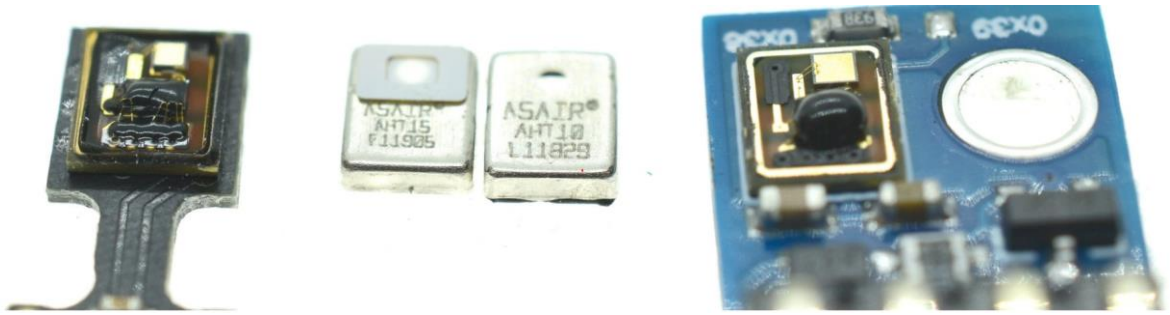

Figure 11 Microscope pictures of the sensors

The pictures below are representing practical productions made specifically for experiments that follow. Furthermore there will be made the experiments and will be compared the characteristics of both of the sensors.

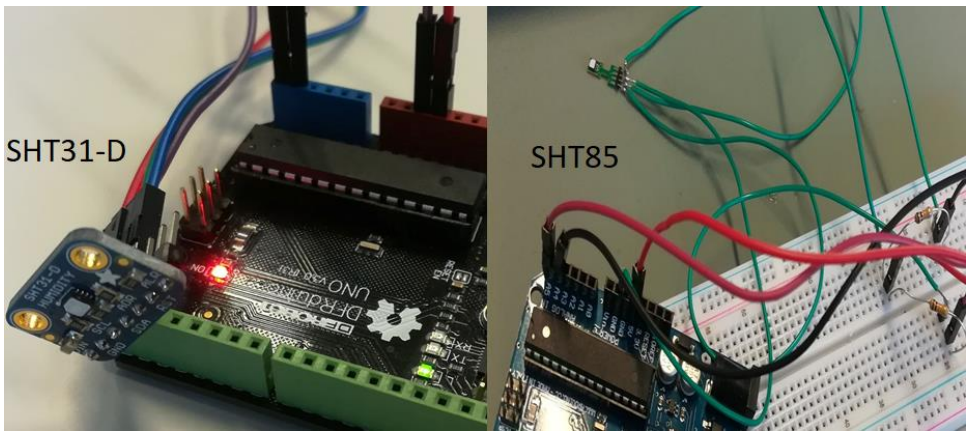

Figure 12 Practical productions

The experiments were done with SHT85, SHT31-D and also a measuring device with 99.8% accuracy. From the picture below is visible that SHT85 is more near by the real value and also it is faster at the normalizing the data flow. The SHT31-D has almost 0.30 degrees Celsius error from the real value and that it does not meet the requirements and needs of the project. Overall SHT85 it is with better characteristics and accuracy. Furthermore this sensor will be used in the building of the prototype.

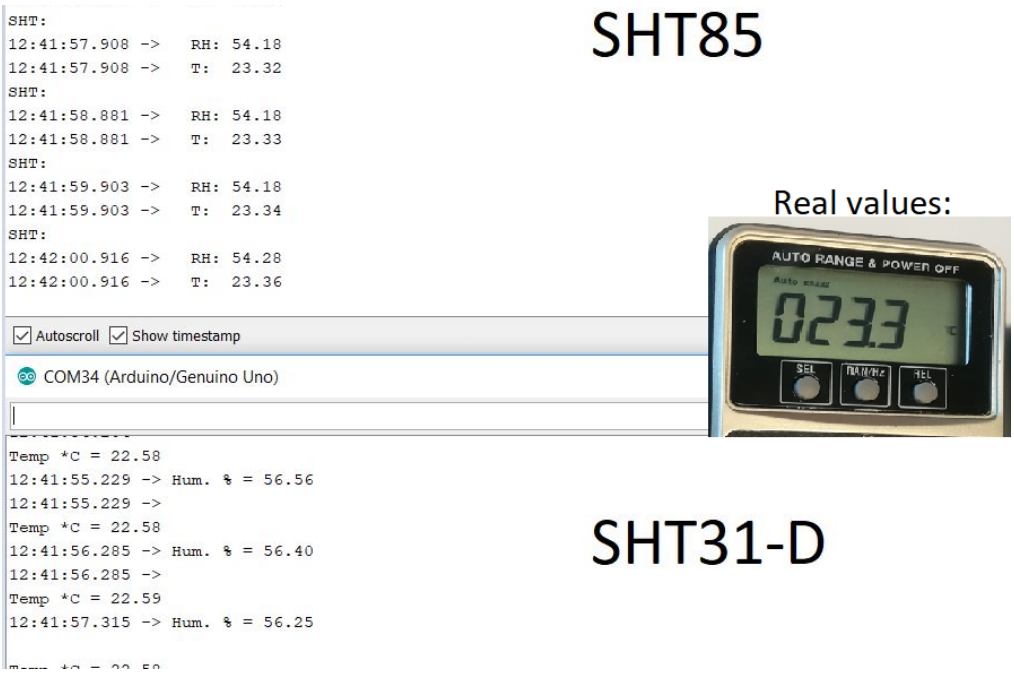

Figure 13 Results from experiments

2. Weight Sensor

The aim of this chapter is to define which sensor is most suitable for the research project. This has been done to up efficiency and the accuracy of the device that will be built.

The sensors are divided on 3 main categories – load cell, strain gauge and force-sensitive resistors. In this research will be test the characteristics and accuracy of two classes that are most accessible to the research team – load cells and FSRs.

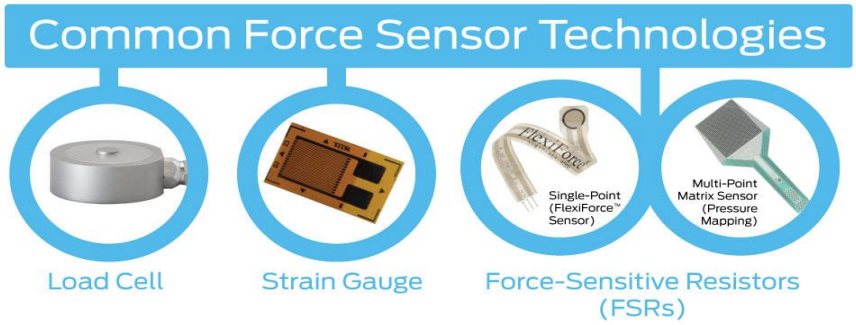

Figure 14 Types of common force sensors

2.1 Load Cell Basics

A load cell is a physical element (or transducer if you want to be technical) that can translate pressure (force) into an electrical signal.

2.1.1 Hydraulic Load Cells

Hydraulic load cells use a conventional piston and cylinder arrangement to convey a change in pressure by the movement of the piston and a diaphragm arrangement which produces a change in the pressure on a Bourdon tube connected with the load cells.

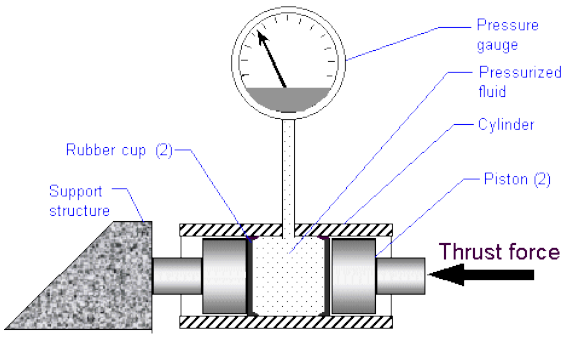

Figure 15 Diagram of a Hydraulic Load Cell [3]

2.1.2 Pneumatic Load Cells

Pneumatic load cells use air pressure applied to one end of a diaphragm, and it escapes through the nozzle placed at the bottom of the load cell, which has a pressure gauge inside of the cell.

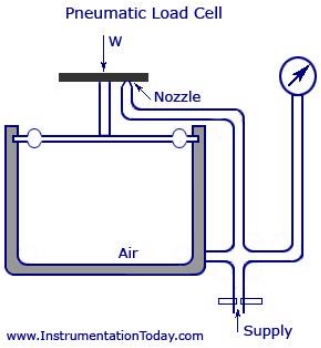

Figure 16 Diagram of a pneumatic load cell [4]

2.1.3 Strain Gauge Load Cells

And lastly (though there are many other less common load cell set ups), there is a strain gauge load cell, which is a mechanical element of which the force is being sensed by the deformation of a (or several) strain gauge(s) on the element.

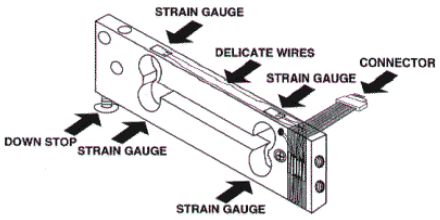

Figure 17 Strain gauge load cell diagram [5]

In bar strain gauge load cells, the cell is set up in a "Z" formations so that torque is applied to the bar and the four strain gauges on the cell will measure the bending distortion, two measuring compression and two tension. When these four strain gauges are set up in a wheatstone bridge formation, it is easy to accurately measure the small changes in resistance from the strain gauges. [5]

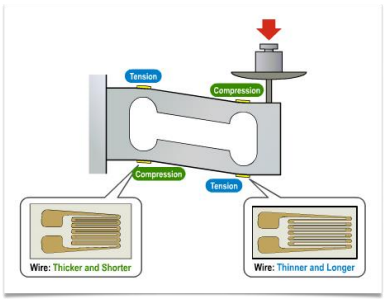

Figure 18 More in depth diagram of strain gauges on bar load cells when force is applied [5]

2.2 Testing and evaluating

2.2.1 Reference research

The experimental setup shown in the picture below was developed to measure the reflection of the hip force. The change in the sensed voltage from the Wheatstone Bridge of the two FSR sensors and the additional two resistances was measured with an AD converter during which a force was provided to the hip force sensing part. Three axis precision stages with a manual positioner that was able to move the sensing part and load cell with a precision of <1 μm were used to apply force to the sensing part with 1 mN resolution. The sensing part contacted the tip of the load cell and force was applied to it in each direction and at each position. b) shows the *z*-axis force measurement setup. Dynamic testing was performed using the measurement setup consisting of repeatedly loading and unloading the sensor 4 times. Identical measurements were performed for force applied to the *z*-, *y*- and *x*-axes [6]

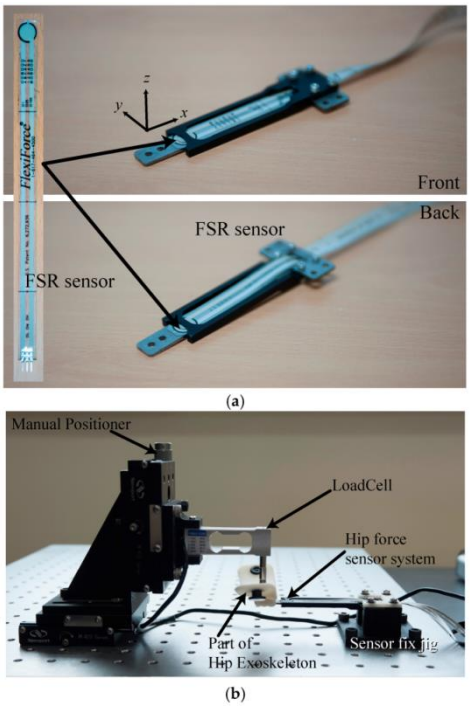

Figure 19 a) The developed sensor system and (b) force measurement and calibration system setup [6].

The picture below shows the experimental results of the relationship between the input force and the voltage variation of each sensor. a, b shows graphs of the relationship between the loading force on the *z*-axis and the measured voltage at the two sensors. For this system's structural characteristics, variation output occurred in one sensor when applying force to the system while the other sensor did not register any change. During the loading stage, the sensors followed the upper curve, while during the unloading stage, they followed the lower side of the curve. Subplot c–e shows graphs of the relationship between the loading force on the *y*- and *x*-axes and the measured voltage at the two sensors. The sensing accuracy is 1.5 N due to the nonlinearity of the FSR sensor and hysteresis of the sensor. The sensing accuracy is

below the Weber fraction, which is allowable for a wearable device, because a human cannot discriminate the force difference. [6]

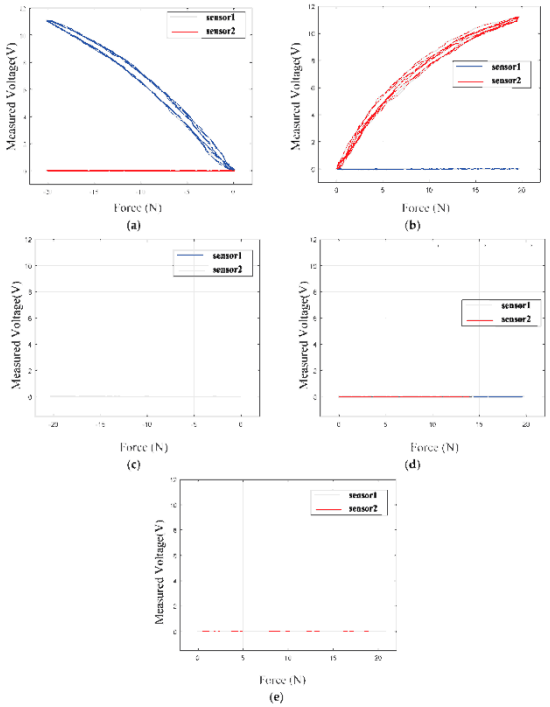

Figure 20 Experimental results of the relationship between the input force on the z-axis (a,b), the y-axis (c,d) and x-axis (e) and the voltage variation of each sensor. [6]

2.2.2 Applying the reference research

The experimentals productions show in the pictures below are the prove of the hypothesis that FSR are not accurate enough and also that the load cell is the only class of weight sensors that meets the requirements of the research.

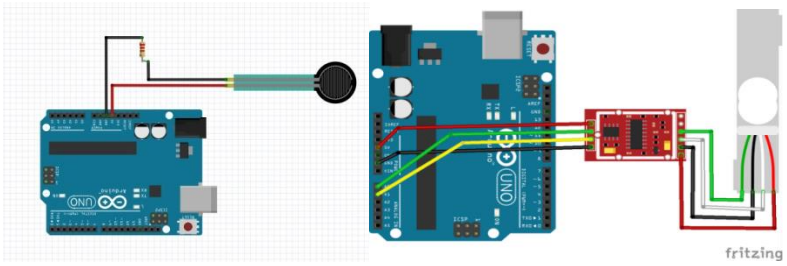

Figure 21 Productions for experiments

2.2.2.1 FSR testing

In the pictures below is show the prototype that was made for testing the FSR . The object that is measured in that case is lighter with around 200-250 grams weight. From the test was finding out that the surface under the FSR sensor was in close relationship with the accuracy.

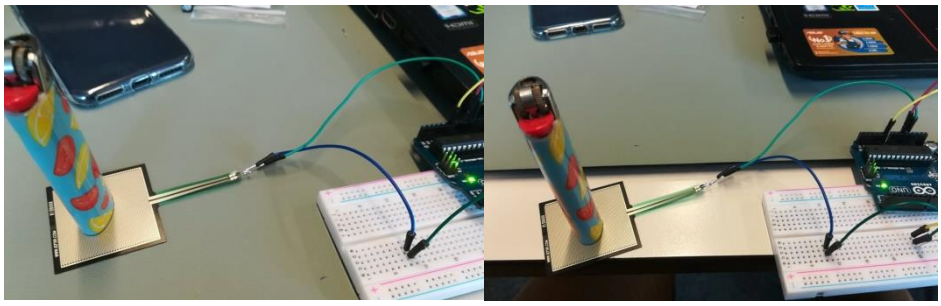

Figure 22 Experiments with FSR

Also the position of the lighter was in relationship with the accuracy of the sensor. Overall the FSR sensor is really not accurate as shown in the picture below because of the nonlinearity of the resistance.

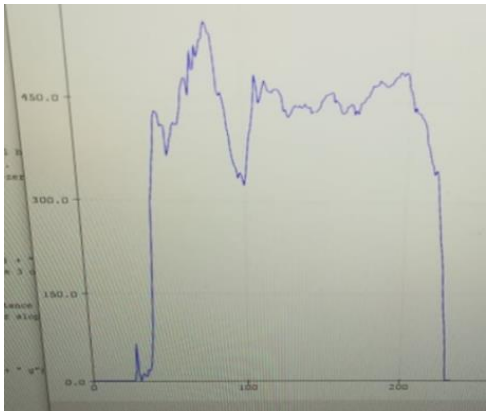

Figure 23 Results from FSR

2.2.2.2 Load cell testing

The object of measurement of the test with the load cell was coin of 10 cent with 34 grams weigh. First experiment was done by measuring the coin in three different states - the moment when the coin was put, moment of stabilizing and normalizing the data and finally when the coin was taken out from the load cell. In the graph below are really visible the three states. And the result is with 99.8% accuracy.

Figure 24 Experiment with load cell and coin

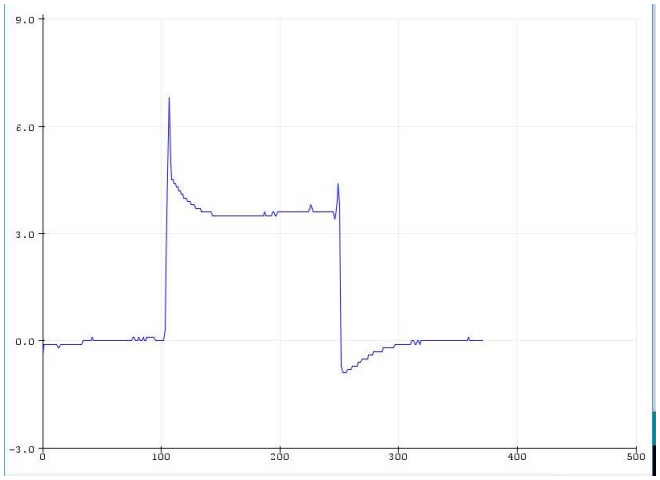

Figure 25 Results from load cell experiment

The second test was made with real predefined REVIT cup to finally test the accuracy of the sensor. And the results from the experiment is proves that this class of sensors are most suitable for this technical research.

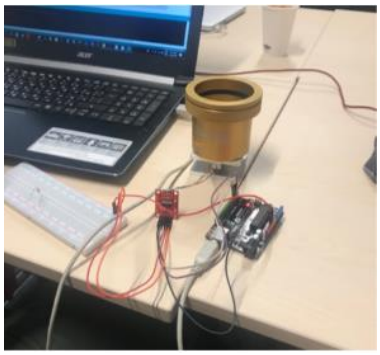

Figure 26 Experiment with REVIT cup

3. Micro controllers

3.1 Arduino UNO

The UNO is arguably the most popular Arduino. It is powered by an Atmega328 processor operating at 16MHz, includes 32KB of program memory, 1KB of EEPROM, 2KB of RAM, has 14 digital I/O, 6 analog inputs, and both 5V and 3.3V power rails.

Figure 27 Arduino UNO [7]

The Arduino UNO has a pin header arrangement that is rapidly becoming the industry standard for development boards, making it compatible with most development board shields on the market.A power jack is included on the UNO, allowing it to be powered by an external wall wart. There is also a VIN option available for connecting the UNO to batteries.The physical dimensions of the UNO (69mm x 54mm) make it a small development board that can easily fit into many projects and the four screw holes allow designers to securely fit them into place.

3.2 Arduino NANO

The Arduino Nano is essentially an Arduino UNO shrunk into a very small profile, making it very convenient for tight spaces and projects that may need to reduce weight wherever possible.Like the UNO, the Nano is powered by an Atmega328 processor operating at 16MHz, includes 32KB of program memory, 1KB of EEPROM, 2KB of RAM, has 14 digital I/O, 6 analog inputs, and both 5V and 3.3V power rails.

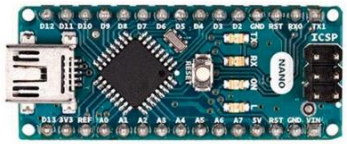

Figure 28 Arduino NANO [7]

The Nano, unlike the UNO, cannot connect to Arduino shields but it has pin headers which make it useful for breadboard prototyping or in PCBs with the use of a socket. Often, Arduino Nano boards are the cheapest Arduino board option available making them cost-effective for larger projects.

3.3 Arduino DUE

The Arduino Due is one of the larger boards and is also the first Arduino board to be powered by an ARM processor.While the UNO and Nano operate at 5V, the Due operates at 3.3V—this is important to note, because overvoltage will irreparably damage the board. Powered by an ATSAM3X8E Cortex-M3 running at 84MHz, the Due has 512KB of ROM and 96KB RAM, 54 digital I/O pins, 12 PWM channels, 12 analog inputs, and 2 analog outputs.

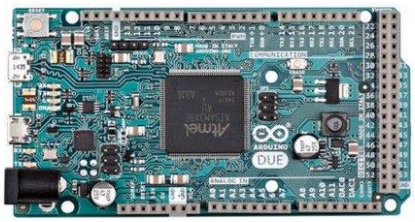

Figure 29 Arduino DUE [7]

The Due does not have any on-board EEPROM and is one of the more expensive Arduino boards. While the Due has a large number of pin headers for connecting to the many digital I/O, it is also pin-compatible with standard Arduino shields. Software compatibility with the Due cannot be guaranteed.

3.4 Arduino MEGA 2560

The Arduino Mega is somewhat similar to the Due in that it also has 54 I/O. However, instead of being powered by an ARM core, it instead uses an ATmega2560.The CPU is clocked at 16MHz and includes 256KB of ROM, 8KB of RAM, 4KB of EEPROM, and operates at 5V making it easy to use with most hobby friendly electronics.

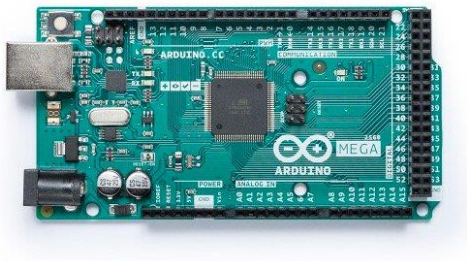

Figure 30 Arduino MEGA [7]

The Arduino Mega has 16 analog inputs, 15 PWM channels, a pinout similar to the Due, and is hardware compatible with Arduino shields. Like the Due, software compatibility with the Mega cannot always be guaranteed.

3.5 Comparison

Arduino code can be easily transferred to different boards with virtually no changes which is highly beneficial to any designers wanting to change their mind about what board their project will use.The deciding factor each project will use comes down to two basic things: hardware and cost. While the cost aspect of each Arduino is obvious (the lowest cost option is always the preference), the hardware may not be so easy to determine. When looking at hardware the following should be considered:

- Physical dimensions
- CPU power
- Memory size
- I/O capabilities
- On-board peripherals
- Weight
- Connectivity

When it comes to physical dimensions the Arduino Nano is the smallest and is a very portable device. The UNO is a medium sized development board but is still small enough to be mounted to many projects including remote-controlled devices such as RC cars and boats. The Mega and Due are much larger boards which makes them difficult to use in space restricted applications.

Board	Best Applications	Example Projects
Arduino Nano	Low cost, small profile, simple projects	RC planes, portable electronics, and sensor gathering
Arduino Uno	Desktop prototyping and use with Arduino shields	Simple robot controller, RC cars, simple games console, IoT sensors, and device testing
Arduino Mega	High I/O requirements with more memory space	DIY bench tools, multi-device controlling, machine controller, home automation
Arduino Due	High performance prototyping with superior analog I/O	Data processor of multiple sources, home automation, machine controller

Figure 31 Comparison table

4. Architecture

The graphic below is representing the basic method of operation of the device that should be built in the end of these technical research. Basically there are 6 sensors for humidity and temperature and 6 sensors that are measuring the weight of the REVIT cup continuously. After that all of them send the raw data to microcontroller. Furthermore the raw data is normalize and is send to the firmware that will be discussed in next chapter.

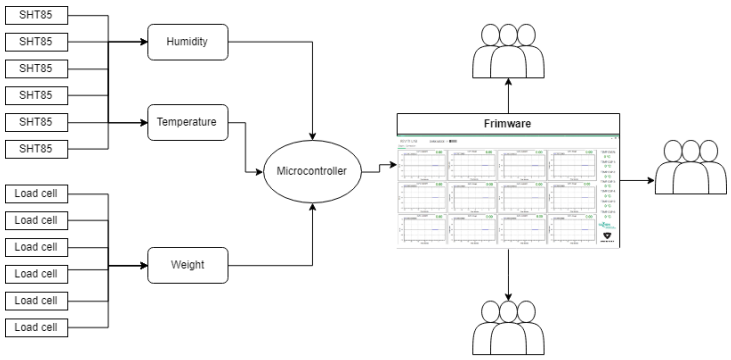

Figure 32 Method of operation

5. Graphical user interface

In the picture below is representing the concept how should look the final firmware. It should represent continuously the humidity and weight levels. Also to make log book of all the data that is received.

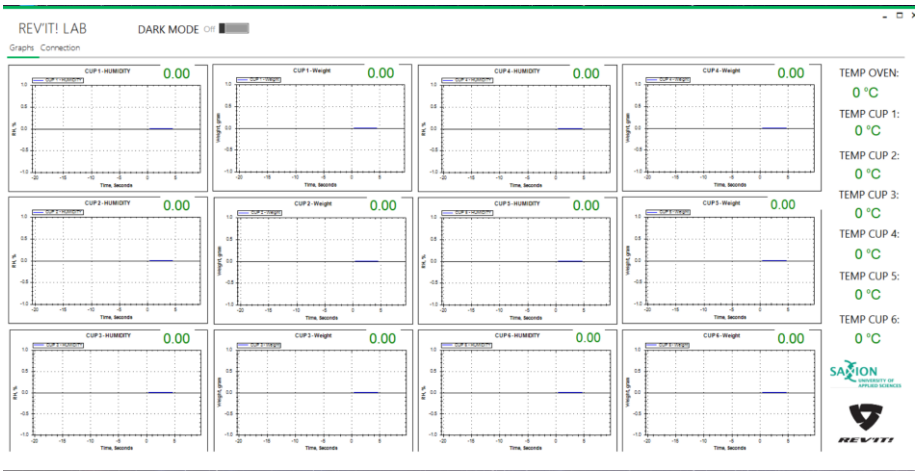

Figure 33 Firmware front page

The firmware has a window for establishing connection with the microcontroller. Also has dark mode that is making all of the components black and white. Only the graphs in dark mode are not going to be black. They will be gray.

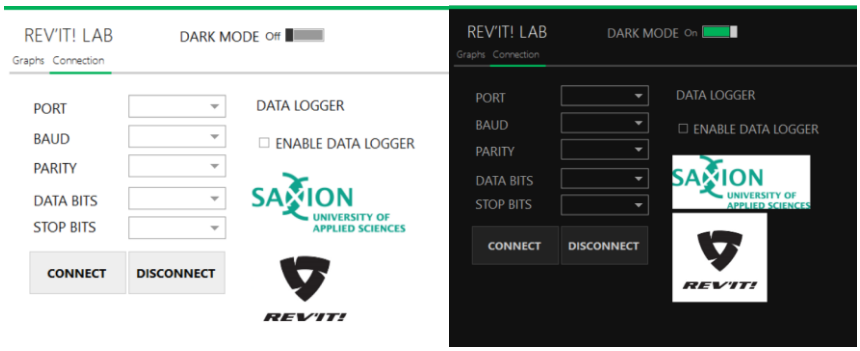

Figure 34 Firmware connection page

6. Bibliography

[1] Liutyi, "Liutyi.info," 2018. [Online]. Available: https://wiki.liutyi.info/.

[2] kandrsmith, "Wide range of Hygrometers," 2018. [Online]. Available: http://www.kandrsmith.org/RJS/Misc/Hygrometers/calib_many.html.

[3] R. N. E. R. W. Site, "Richard Nakka's Experimental Rocketry Web Site," [Online]. Available: http://www.nakka-rocketry.net/hydlc.html.

[4] F. Transducers, "instrumentationtoday," [Online]. Available: http://www.instrumentationtoday.com/force-transducers/2011/07/.

[5] scalenet, "scalenet," [Online]. Available: http://www.scalenet.com/applications/glossary.html.

[6] Samsung-ro, Yeongtong-gu, Suwon-si, "Compact Hip-Force Sensor for a Gait-Assistance Exoskeleton System," [Online]. Available: https://www.mdpi.com/1424-8220/18/2/566/htm.

[7] Arduino. [Online]. Available: https://www.arduino.cc.